Topological states in a non-Hermitian two-dimensional Su-Schrieffer-Heeger model

C. Yuce [1,*] and H. Ramezani[2]

[1]*Department of Physics, Eskisehir Technical University, Eskisehir, Turkey*
[2]*Department of Physics and Astronomy, University of Texas Rio Grande Valley, Brownsville, Texas 78520, USA*

A non-Hermitian topological insulator with a real spectrum is interesting in the theory of non-Hermitian extension of topological systems. We find an experimentally realizable example of a two-dimensional non-Hermitian topological insulator with a real spectrum. We consider the two-dimensional Su-Schrieffer-Heeger (SSH) model with gain and loss. We introduce a non-Hermitian polarization vector to explore topological phase and show that topological edge states in the band gap exist in the system.

I. INTRODUCTION

The past few years have witnessed a growing amount of interest in the theory of non-Hermitian extension of topological insulators [1,2]. A combination of long-lived quantum states immune to decoherence and the unique features of non-Hermitian systems make non-Hermitian topological systems a promising platform for future applications in quantum technology. One cannot directly generalize the standard theory of topological insulators to non-Hermitian systems since they do not always have real eigenvalues and orthogonal eigenstates. Furthermore, exceptional points (EPs), where at least two eigenstates coalesce, can appear only in non-Hermitian systems [3] and can lead to new topological features. This field of study is still in its infancy and non-Hermitian topological phases have been mainly investigated in one-dimensional (1D) topological systems such as Su-Schrieffer-Heeger (SSH) lattices [4–18], Aubry-Andre chain [19], and Kitaev model [20–24], in which non-Hermiticity is obtained by introducing asymmetric tunneling amplitudes and/or gain-loss.

The standard bulk-boundary correspondence does not work in non-Hermitian systems [25–32]. The so-called non-Hermitian skin effect arises when the topological lattice has asymmetric tunneling amplitudes. In this case, bulk states as well as topological states are localized near edges. In contrast to Hermitian systems, topological phase transition points cannot be determined by the translationally invariant form of the non-Hermitian Hamiltonian. We stress that topological phase transition can also be induced solely by gain and loss [33]. Recently, the idea of pseudotopological insulators has been introduced to explain topological edge states for massive SSH Hamiltonian [34].

There is a fundamental difference between the Hermitian and non-Hermitian one-dimensional (1D) topological insulating systems. In topologically nontrivial Hermitian systems, edge states disappear when the band gap is closed. However, edge states may acquire an imaginary energy gap in non-Hermitian systems. The complex topological state can be used

to generate spontaneous topological pumping [35] and topological lasing [36,37]. The existence of complex topological states in non-Hermitian systems has applications in lasing and is of special importance, yet it is a nontrivial task is to find topological edge states with real eigenvalues in non-Hermitian systems. It was theoretically shown in Ref. [19] that such states exist in a complex extension of the Aubry-Andre model. Topological zero-energy edge state in a 1D photonic lattice was experimentally realized [38]. However, no non-Hermitian topological system with real spectrum has been found in the literature in two dimensions (2D) [39–51]. It is tempting to find topological systems with real eigenvalues in 2D. In this paper, we consider the two-dimensional Su-Schrieffer-Heeger (SSH) model with gain and loss, which can be experimentally realized with current technology in photonics. In the absence of gain and loss, a nontrivial topological phase was shown to exist even if the Berry curvature is zero [52,53]. In the presence of gain and loss, we show that the system can have real valued energy eigenvalues for all bulk and topological states. We introduce complex polarization vector and discuss topological invariant in our non-Hermitian system.

II. THE 2D SSH MODEL

Consider the 2D Su-Schrieffer-Heeger model with gain and loss, which describes a non-Hermitian square lattice with alternating tunneling amplitudes in each direction. The tunneling amplitudes in horizontal and vertical directions are assumed to be alternating between ω and ν, as shown in Fig. 1. There are four sites in the unit cell and one can add gain and loss in the unit cell. The non-Hermitian Hamiltonian we consider is given by

$$\mathcal{H} = \sum_{i,j} \Delta_i \, a_{i+1,j}^\dagger \, a_{i,j} + \Delta_j \, a_{i,j+1}^\dagger \, a_{i,j}$$
$$+ i \sum_{i,j} \gamma_{ij} \, a_{i,j}^\dagger \, a_{i,j} + \text{H.c.,} \quad (1)$$

where $a_{i,j}^\dagger$ and $a_{i,j}$ are the creation and annihilation operators at the site (i, j), respectively, $\Delta_{i,j} = t + (-1)^{i,j} \delta, t > 0$ is the reference tunneling amplitude, and $\delta < t$ is a constant, which
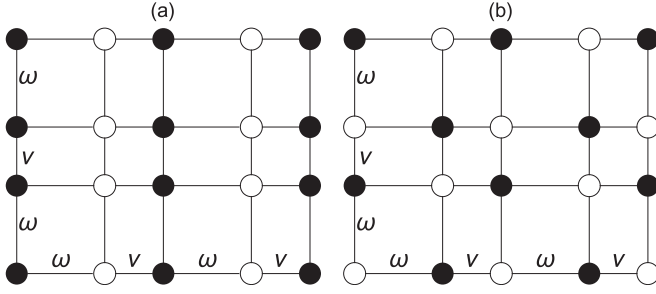
*cyuce@eskisehir.edu.tr

FIG. 1. A square lattice with alternating tunneling amplitudes ω and ν in each direction. Black circles have gain while unfilled circles have loss. The corresponding non-Hermitian Hamiltonians are given by (3). The gain and loss impurities alternate only in the horizontal (x) direction in panel (a) while they alternate in both horizontal and vertical (y) directions in panel (b). The corresponding energy bands can be real for panel (a) unless the non-Hermitian degree does not exceed a critical number. However, they are complex for panel (b) for any nonzero value of the non-Hermitian degree.
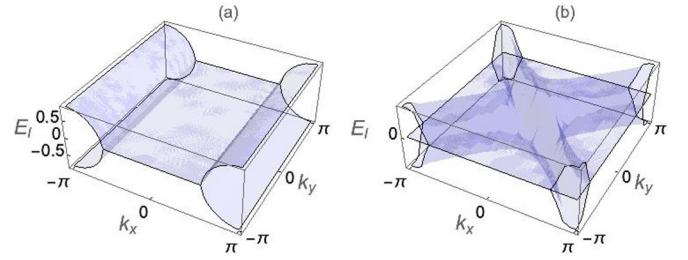

FIG. 2. Imaginary part of energy eigenvalue for the system depicted in Fig. 1(a) at $\gamma = 1$ (a) and Fig. 1(b) at $\gamma = 0.2$ (b). The tunneling amplitudes are given by $\nu = 1$ and $\omega = 0.5$. The system in panel (a) has a real spectrum unless $\gamma > |\nu - \omega|$ while the system in panel (b) has a complex spectrum whenever $\gamma \neq 0$.

are related to the tunneling amplitudes through $\omega = t - \delta$ and $\nu = t + \delta$ and the real valued parameters γ_{ij} describe gain-loss strengths at the lattice sites i, j. We consider that the system is periodic and hence the gain-loss strengths in the unit cell are given by $\{\gamma_1, \gamma_2, \gamma_3, \gamma_4\}$. Here, we assume that the gain and loss in the system is balanced, which implies $\gamma_1 + \gamma_2 + \gamma_3 + \gamma_4 = 0$.

The gain and loss can be arranged in various ways in the unit lattice. Figure 1 depicts two such configurations where black and white circles denote gain and loss impurities. The non-Hermitian strengths in the unit cell are given by $\{\gamma, -\gamma, \gamma, -\gamma\}$ and $\{-\gamma, \gamma, \gamma, -\gamma\}$ for 1(a) and 1(b), respectively, where γ is a constant. In both cases, the systems have balanced gain and loss. We stress that the reality of the spectrum depends sensitively on the gain and loss arrangements in the system.

Applying the Fourier transformation, we get the matrix form of the Hamiltonian in the **k**-space

$$\mathcal{H} = \begin{pmatrix} i\gamma_1 & \omega + \nu e^{-ik_x} & \omega + \nu e^{-ik_y} & 0 \\ \omega + \nu e^{ik_x} & i\gamma_2 & 0 & \omega + \nu e^{-ik_y} \\ \omega + \nu e^{ik_y} & 0 & i\gamma_3 & \omega + \nu e^{-ik_x} \\ 0 & \omega + \nu e^{ik_y} & \omega + \nu e^{ik_x} & i\gamma_4 \end{pmatrix}.$$
(2)

To study symmetry properties of the two choices in Fig. 1, we rewrite the corresponding Hamiltonians using the Pauli spin matrices. If we specify the gain and loss strengths in the unit cell, we get

$$\mathcal{H}_1 = \mathcal{H}_0 + i\gamma\, \mathcal{I} \otimes \sigma_z,$$
$$\mathcal{H}_2 = \mathcal{H}_0 - i\gamma\, \tau_z \otimes \sigma_z,$$
(3)

where $\mathcal{I}$ is the identity matrix and their Hermitian part $\mathcal{H}_0$ reads

$$\mathcal{H}_0 = (\omega + \nu \cos k_x)\,\mathcal{I} \otimes \sigma_x - \nu \sin k_x\,\mathcal{I} \otimes \sigma_y$$
$$+ (\omega + \nu \cos k_y)\,\tau_x \otimes \mathcal{I} + \nu \sin k_y\,\tau_y \otimes \mathcal{I}.$$
(4)

The Hermitian Hamiltonian $\mathcal{H}_0$ has both inversion and time-reversal symmetries, which lead to zero Berry curvature everywhere in the Brillouin zone, except at band-gap closing points. Note that the inversion operator inverts momenta $\mathbf{k} \to -\mathbf{k}$ and is given by $\tau_x \otimes \sigma_x$. The time-reversal operator reads $\mathcal{T} = \mathcal{I} \otimes \mathcal{I}\mathcal{K}$, where $\mathcal{K}$ is the complex conjugation operator. The inversion symmetry remains intact only for the non-Hermitian Hamiltonian $\mathcal{H}_2$. However, the time-reversal symmetry is lost for both $\mathcal{H}_1$ and $\mathcal{H}_2$. It is interesting to see that only $\mathcal{H}_1$ has combined parity-time symmetry $\mathcal{PT} = \tau_x \otimes \sigma_x \mathcal{K}$. Therefore, energy bands for $\mathcal{H}_1$ are real-valued unless the $\mathcal{PT}$ symmetry is spontaneously broken. To this end, we note that both $\mathcal{H}_1$ and $\mathcal{H}_2$ have particle-hole symmetry $\mathcal{C} = \tau_z \otimes \sigma_z \mathcal{K}$. This implies that energy eigenvalues are symmetric with respect to the zero energy line.

Let us now study their spectra. There are four energy bands since there are four sites in the unit cell. In the absence of gain and loss, the lowest and highest bands are isolated while the middle two bands touch each other at momenta (0,0), $(\mp\pi, \mp\pi)$ and $(\pm\pi, \mp\pi)$. The band gap between the lowest (highest) two bands decreases with decreasing $|\omega - \nu|$ and closes at $\omega = \nu$, where all four bands touch at the edges of the Brillouin zone. This is a signature of topological phase transition. In the non-Hermitian case, the gain and loss arrangements in the lattice plays a vital role on the reality of the spectrum. The non-Hermitian Hamiltonian $\mathcal{H}_1$ has complex eigenvalues when $|\gamma| > \gamma_c = |\nu - \omega|$ while $\mathcal{H}_2$ has complex eigenvalues for any nonzero value of γ. In Figs. 2(a) and 2(b), we plot the imaginary parts of energy eigenvalues for $\mathcal{H}_1$ at $\gamma = 1 > \gamma_c$ and $\mathcal{H}_2$ at $\gamma = 0.2$, respectively. Below, we will focus on $\mathcal{H}_1$ as we are interested in finding topological states with real eigenvalues. In this case, increasing γ at fixed ω and ν decreases the band gap between the lowest (highest) two bands and close them at the edges of the Brillouin zone at $\gamma = \gamma_c$. Beyond this value, complex eigenvalues appear around the band edges. We see that the imaginary part of the eigenvalues in **k**-space has the shape of half-elliptic cylinder identically centered at $k_x = \mp\pi$, as can be seen from Fig. 2(a). Its length is fixed to 2π in the k_y direction but its semiaxis in the k_x direction increases with increasing γ. For large values of γ, these two shapes merge and then the spectrum becomes complex valued in the whole **k**-space. To understand band gap opening and closing better, let us now vary ω at fixed

ν and γ. The system is gapped and has real eigenvalues for large values of ω. The band gap is decreased with decreasing ω and the two bands are closed at $\omega = \nu + \gamma$. In this case, exceptional points occur at the band edges. If we decrease ω further, the band gap does not reopen. Instead, exceptional points (which separate the region of complex and real-valued eigenvalues in **k**-space) move in the **k**-space until $\omega = \nu - \gamma$, at which a pair of exceptional points annihilate each other and the spectrum becomes real valued again. Generally speaking, one cannot explore topological phase transition in a non-Hermitian system just by studying band-gap closing and reopening. To study topological features in the system, we need to find the corresponding topological invariant. In the absence of gain and loss, the Berry curvature vanishes due to inversion and time-reversal symmetries. In the presence of gain and loss, time-reversal symmetry is broken for both $\mathcal{H}_1$ and $\mathcal{H}_2$. However, this does not necessarily mean that the Chern number is quantized to be an integer multiple. Generally speaking, the standard definition of Chern number does not work in non-Hermitian systems. So, we need to introduce a new topological number. Below, we study this issue.

III. COMPLEX POLARIZATION VECTOR

The polarization (electric dipole moment per unit volume) in a periodical potential such as a solid is not uniquely defined, which leads to ambiguity for the value of the dielectric displacement field. Fortunately, not the absolute value but the change in polarization can be measured in a real experiment. In 1993 [54], King-Smith and Vanderbilt formulated the polarization vector. The polarization vector is also of special importance in the theory of topological insulators [55]. In Refs. [52,53], the authors used a polarization vector to discuss the topological phase in a 2D Hermitian SSH system, where the Berry curvature is zero. Unfortunately, the standard polarization vector is not quantized in our non-Hermitian system, where inversion and time-reversal symmetries are broken. In fact, one cannot directly apply the Hermitian polarization vector to a non-Hermitian system because of the nonorthogonal character of eigenstates in non-Hermitian systems. Our aim is to find its complex generalization.

Let us introduce the left-right and right-left non-Hermitian polarization vectors. The contributions from the nth band read

$$\mathbf{P}_n^{LR} = \frac{e}{(2\pi)^2} \int dk_x dk_y \langle \psi_n^L | i\partial_{\mathbf{k}} | \psi_n^R \rangle,$$

$$\mathbf{P}_n^{RL} = \frac{e}{(2\pi)^2} \int dk_x dk_y \langle \psi_n^R | i\partial_{\mathbf{k}} | \psi_n^L \rangle, \qquad (5)$$

where the integral is taken over the 2D Brillouin zone, n labels the band index, and $|\psi_n^R\rangle$, $|\psi_n^L\rangle$ are the normalized right and left eigenvectors of the Hamiltonian, which form a biorthogonal basis $\langle \psi_n^L | \psi_m^R \rangle = \delta_{nm}$. Below, we set the charge $e = 1$. Note that inversion and time-reversal symmetries are not required in the calculation of the non-Hermitian polarization vector. We assume that the band is gapped. The non-Hermitian polarization vector is not well defined at the EP since $\langle \psi_n^L | \psi_n^R \rangle$ vanishes at the EP.
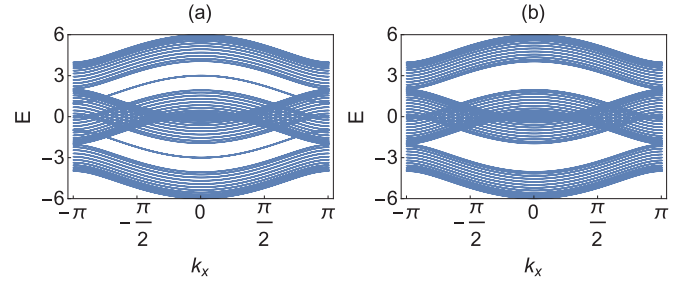

FIG. 3. The spectra for the Hermitian system periodic along the x direction has $N_y = 52$ sites in the y direction. The parameters are $\omega = 1$, $\nu = 2$ (a) and $\omega = 2$ $\nu = 1$ (b). Topological edge states appear in the band gap in panel (a).

Using the condition $\langle \psi_n^L | \psi_n^R \rangle = 1$, one can see that $\langle \psi_n^L | i\partial_{\mathbf{k}} \psi_n^R \rangle = -\langle i\partial_{\mathbf{k}} \psi_n^L | \psi_n^R \rangle = (\langle \psi_n^R | i\partial_{\mathbf{k}} \psi_n^L \rangle)^\star$. This implies that $\mathbf{P}_n^{LR} = (\mathbf{P}_n^{RL})^\star$. As a result, we define the real-valued total non-Hermitian polarization vector in a two-dimensional non-Hermitian gapped system as

$$\mathbf{P} = \sum_n^{occ} \frac{\mathbf{P}_n^{LR} + \mathbf{P}_n^{RL}}{2}, \qquad (6)$$

where the summation is over the occupied states.

We calculate the non-Hermitian polarization vector for the lowest-lying eigenstate of the Hamiltonian $\mathcal{H}_1$. It is quantized and equal to $\mathbf{P}_1 = (1/2, 1/2)$ for $\nu > \omega + |\gamma|$ and $(0,0)$ for otherwise. We can define the two-dimensional complex Berry (Zak) phase for the nth band as $2\pi \mathbf{P}_n$. It is quantized and a topological invariant. In other words, adiabatic deformations of the Hamiltonian $\mathcal{H}_1$ do not change it as long as the band gap is preserved. To this end, we note that the imaginary parts of $\mathbf{P}_n^{RL}$ cancel each other for the first (and last) two bands in pairs and their sum is also quantized. We get $\mathbf{P}_1^{LR} + \mathbf{P}_2^{LR} = (1, 1)$ and $\mathbf{P}_3^{LR} + \mathbf{P}_4^{LR} = 1$ for $\nu > \omega + |\gamma|$. In Ref. [44], four different gauge-invariant Berry curvatures are constructed using the combination of right and left eigenstates and the corresponding four Chern numbers are shown to be equal to each other. The above complex polarization vector is different from the complex Chern number introduced in Ref. [44].

Having discussed the topological invariant, we are now in position to study topological edge states. To see them, we plot the energy spectra for a ribbon periodic along the x direction and $N = 52$ sites in the y direction. Consider first the Hermitian case $\gamma = 0$. The energy spectra of the Hermitian system for the nontrivial ($\omega = 1$, $\nu = 2$) and trivial ($\omega = 2$, $\nu = 1$) phases are displayed in Figs. 3(a) and 3(b), respectively. As can be seen from the figure, there is a distinguishing difference between them. The two energy curves within the band gaps appear in the topologically nontrivial case [Fig. 3(a)], while no such curves exist in the trivial case [Fig. 3(b)]. They are, in fact, for the topological edge states. The edge states are doubly degenerate, so there are four topological edge states.

Suppose next that $\gamma \neq 0$. The complex polarization vector predicts the appearance of topological edge states. We perform a numerical computation to plot the spectrum for the same nontrivial system described above but with $\gamma = 0.5$, $\gamma = 1$, and $\gamma = 1.5$ in Fig. 4. One can see the topological
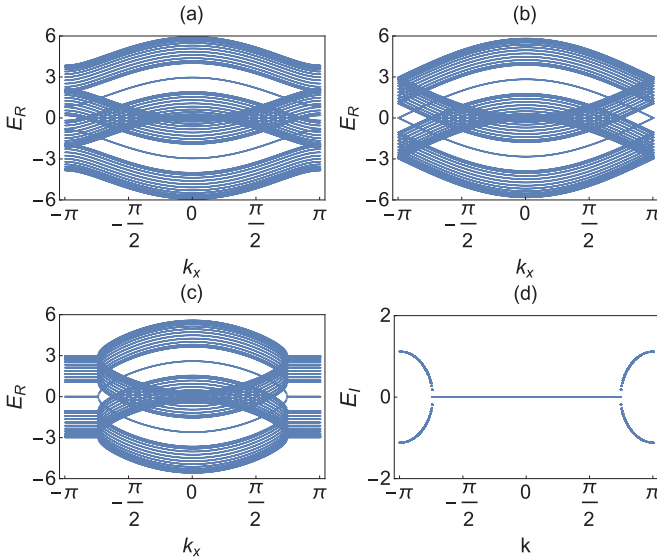
FIG. 4. The non-Hermitian system $\mathcal{H}_1$ periodic along the x direction has $N_y = 52$ sites in the y direction for $\omega = 1$ $\nu = 2$. The real part of the energy band for $\gamma = 0.5$ (a), $\gamma = 1$ (b), and $\gamma = 1.5$ (c) and the corresponding imaginary part for $\gamma = 1.5$ (d). The spectrum becomes complex when $\gamma > 1$.

edge states in the band gap for all three cases. These are doubly degenerate real-valued topological states. Generally speaking, periodical and open boundary conditions do not predict the same critical point γ_c for the transition from real to complex spectrum in a non-Hermitian topological system. Fortunately, this is not the case here. Therefore, the spectra are real in Figs. 4(a) and 4(b) while it is complex around band edges in Fig. 4(c). One can also see that the spectra are

symmetric with respect to the $E = 0$ line. This is because of the particle-hole symmetry of the system.

There is a fundamental difference between the Hermitian and non-Hermitian systems. In the Hermitian SSH, topological edge states disappear whenever the band gap is zero, which occurs at $\nu = \omega$. However, this is not the case in the non-Hermitian system. At $\gamma = \gamma_c = |\nu - \omega|$, the gap vanishes at $k_x = \mp\pi$, as can be seen from Fig. 4(b). In other words, exceptional points occur at $\gamma = \gamma_c$ and $k_x = \mp\pi$. Topological edge states still exist even if $\gamma > \gamma_c$, as can be seen from Fig. 4(c). They have purely imaginary eigenvalues in between $k_x \in [\mp\pi, \mp k_c]$, where k_c increases with γ. For very large values of the non-Hermitian strength, $\gamma > \nu + \omega$, the eigenvalues become purely imaginary in the whole k_x-space. The complex Zak phase based on the non-Hermitian polarization vector predicts the appearance of topological edge states correctly as long as $\gamma \leqslant \gamma_c$. However, it does not work if $\gamma > \gamma_c$ since the band gap is closed in this case. Note that the non-Hermitian polarization vector works only for gapped Hamiltonian. To this end, we say that topological edge states appear also for the other Hamiltonian $\mathcal{H}_2$, but they have purely imaginary eigenvalues. This means that it can be used as a prototype for topological laser in 2D.

To sum up, we have studied a non-Hermitian square lattice, which can be experimentally realized in photonics using waveguides. The corresponding Hamiltonian is a complex extension of the 2D SSH Hamiltonian. We have shown that topological edge states with real eigenvalues appear in the system as long as the non-Hermitian strength is below than a critical value. We have introduced a non-Hermitian polarization vector, which predicts the topological edge states when the spectrum is real. We have shown that topological edge states survive even when the Hamiltonian is gapless.

[1] A. Ghatak and T. Das, J. Phys.: Condens. Matter **31**, 263001 (2019).

[2] V. M. Martinez Alvarez, J. E. Barrios Vargas, M. Berdakin, and L. E. F. Foa Torres, Eur. Phys. J. Special Topics **227**, 1295 (2018).

[3] T. Kato, *Perturbation Theory for Linear Operators* (Springer-Verlag, Berlin, 1966).

[4] L. Jin, Phys. Rev. A **96**, 032103 (2017).

[5] C. Yin, H. Jiang, L. Li, R. Lu, and S. Chen, Phys. Rev. A **97**, 052115 (2018).

[6] C. Yuce, Phys. Rev. A **98**, 012111 (2018).

[7] C. Yuce and Z. Oztas, Sci. Rep. **8**, 17416 (2018).

[8] S. K. Gupta *et al.*, arXiv:1803.00794.

[9] L. Jin, P. Wang, and Z. Song, Sci. Rep. **7**, 5903 (2017).

[10] K. Ding, Z. Q. Zhang, and C. T. Chan, Phys. Rev. B **92**, 235310 (2015).

[11] C. W. Ling, K. H. Choi, T. C. Mok, Z. Q. Zhang, and K. H. Fung, Sci. Rep. **6**, 38049 (2016).

[12] L.-J. Lang, Y. Wang, H. Wang, and Y. D. Chong, Phys. Rev. B **98**, 094307 (2018).

[13] M. Pan, H. Zhao, P. Miao, S. Longhi, and L. Feng, Nat. Commun. **9**, 1308 (2018).

[14] X. Z. Zhang and Z. Song, Phys. Rev. A **99**, 012113 (2019).

[15] B. X. Wang and C. Y. Zhao, Phys. Rev. B **98**, 165435 (2018).

[16] S. Lieu, Phys. Rev. B **97**, 045106 (2018).

[17] Z.-Z. Li, X.-S. Li, L.-L. Zhang, and W.-J. Gong, arXiv:1901.10688.

[18] B. Midya and L. Feng, Phys. Rev. A **98**, 043838 (2018).

[19] C. Yuce, Phys. Lett. A **379**, 1213 (2015).

[20] C. Yuce, Phys. Rev. A **93**, 062130 (2016).

[21] C. Li, X. Z. Zhang, G. Zhang, and Z. Song, Phys. Rev. B **97**, 115436 (2018).

[22] M. Klett, H. Cartarius, D. Dast, J. Main, and G. Wunner, Phys. Rev. A **95**, 053626 (2017).

[23] K. Kawabata, Y. Ashida, H. Katsura, and M. Ueda, Phys. Rev. B **98**, 085116 (2018).

[24] H. Menke and M. M. Hirschmann, Phys. Rev. B **95**, 174506 (2017).

[25] V. M. Martinez Alvarez, J. E. Barrios Vargas, and L. E. F. Foa Torres, Phys. Rev. B **97**, 121401(R) (2018).

[26] F. K. Kunst, E. Edvardsson, J. C. Budich, and E. J. Bergholtz, Phys. Rev. Lett. **121**, 026808 (2018).

[27] S. Yao and Z. Wang, Phys. Rev. Lett. **121**, 086803 (2018).

[28] S. Yao, F. Song, and Z. Wang, Phys. Rev. Lett. **121**, 136802 (2018).

[29] C. Yuce, Phys. Rev. A **97**, 042118 (2018).

[30] D. Leykam, K. Y. Bliokh, C. Huang, Y. D. Chong, and F. Nori, Phys. Rev. Lett. **118**, 040401 (2017).

[31] L. Jin and Z. Song, Phys. Rev. B **99**, 081103(R) (2019).

[32] K. Yokomizo and S. Murakami, Phys. Rev. Lett. **123**, 066404 (2019).

[33] K. Takata and M. Notomi, Phys. Rev. Lett. **121**, 213902 (2018).

[34] C. Yuce, Phys. Let. A **383**, 248 (2019).

[35] C. Yuce, Phys. Rev. A **99**, 032109 (2019).

[36] G. Harari *et al.*, Science **359**, eaar4003 (2018).

[37] Y. Ota, R. Katsumi, K. Watanabe, S. Iwamoto, and Y. Arakawa, Commun. Phys. **1**, 86 (2018).

[38] S. Weiman *et al.*, Nat. Mater. **16**, 433 (2017).

[39] Z. Oztas and C. Yuce, Phys. Rev. A **98**, 042104 (2018).

[40] M. Kremer, T. Biesenthal, L. J. Maczewsky, M. Heinrich, R. Thomale, and A. Szameit, Nat. Commun. **10**, 435 (2019).

[41] X.-Y. Zhu, S. K. Gupta, X.-C. Sun, C. He, G.-X. Li, J.-H. Jiang, X.-P. Liu, M.-H. Lu, and Y.-F. Chen, Opt. Express **26**, 24307 (2018).

[42] K. Kawabata, K. Shiozaki, and M. Ueda, Phys. Rev. B **98**, 165148 (2018).

[43] R. Wang, X. Z. Zhang, and Z. Song, Phys. Rev. A **98**, 042120 (2018).

[44] H. Shen, B. Zhen, and L. Fu, Phys. Rev. Lett. **120**, 146402 (2018).

[45] Z. Ozcakmakli Turker and C. Yuce, Phys. Rev. A **99**, 022127 (2019).

[46] H. Wang, J. Ruan, and H. Zhang, Phys. Rev. B **99**, 075130 (2019).

[47] J. C. Budich, J. Carlstrom, F. K. Kunst, and E. J. Bergholtz, Phys. Rev. B **99**, 041406(R) (2019).

[48] K. Moors, A. A. Zyuzin, A. Y. Zyuzin, R. P. Tiwari, and T. L. Schmidt, Phys. Rev. B **99**, 041116(R) (2019).

[49] K. Luo, J. Feng, Y. X. Zhao, and R. Yu, arXiv:1810.09231.

[50] T. Yoshida, R. Peters, N. Kawakami, and Y. Hatsugai, Phys. Rev. B **99**, 121101(R) (2019).

[51] Z. Yang and J. Hu, Phys. Rev. B **99**, 081102(R) (2019).

[52] F. Liu and K. Wakabayashi, Phys. Rev. Lett. **118**, 076803 (2017).

[53] F. Liu, H. Y. Deng, and K. Wakabayashi, Phys. Rev. B **97**, 035442 (2018).

[54] R. D. King-Smith and D. Vanderbilt, Phys. Rev. B **47**, 1651(R) (1993).

[55] W. A. Benalcazar, B. A. Bernevig, and T. L. Hughes, Science **357**, 61 (2017).